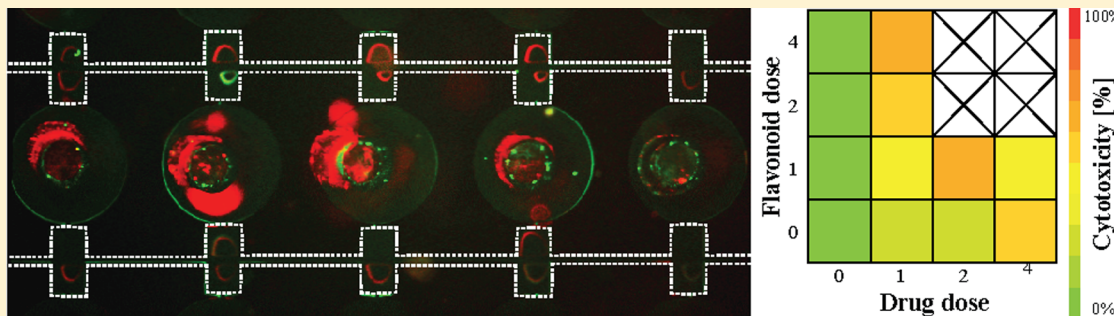


Direct Drug Cocktail Analyses Using Microscale Vortex-Assisted Electroporation

Dwayne A. L. Vickers, Mengxing Ouyang, Chris Hyunseok Choi, and Soojung Claire Hur*

The Rowland Institute at Harvard University, 100 Edwin H. Land Boulevard, Cambridge, Massachusetts 02142, United States

 Supporting Information



ABSTRACT: Combination therapy has become one of the leading approaches for treating complex diseases because it coadministers clinically proven drugs to concurrently target multiple signaling pathways of diseased cells. Identification of synergic drug combinations at their respective effective doses without unwanted accumulative side effects is the key to success for such therapy. In this work, we demonstrate the feasibility of the vortex-assisted microfluidic electroporation system for direct drug cocktail analyses where drug substances were individually delivered into cytosols in a sequential and dosage-controlled manner. Through quantitative analyses, the synergic combinational dosage ratios of the chemotherapeutic drug and the anticancer flavonoid were identified. When integrated with high-throughput label-free rare cell purification techniques, the presented system has the potential for development of personalized medicines as the system would be capable of comprehensively assessing drug combinations directly on patients' cellular samples.

Combination drug therapy has been proposed as a treatment strategy for complex diseases such as cancer,¹ HIV,² cardiovascular disease,³ and type 2 diabetes.⁴ For such therapy, two or more already-licensed drugs are simultaneously administered to maximize therapeutic drug efficacy by targeting multiple signaling pathways while minimizing overlapping toxicity and inhibiting resistance-developing mechanisms.^{5–7} Due to its therapeutic benefits, extensive efforts have focused on the discovery of new drug combinations that work synergistically. For newly discovered drug combinations to rapidly progress to the clinic, systematic unbiased drug-screening strategies should complement existing hypothesis-driven approaches.⁸ However, identification of respective doses for individual agents that induce synergistic therapeutic outcomes is an essential but challenging task. Consequently, these drug combination screenings are very laborious; thus, the use of high-throughput liquid dispensing systems is inevitable for processing time reduction and precision improvement.⁹ However, not only do such systems have high fixed and operating costs,¹⁰ but their assay performances also are susceptible to noises and variations inherent in cell-based microplate assays.¹¹ Furthermore, a real dose–response curve and the cytotoxicity of drug combinations cannot be revealed if administered drugs have widely diverse physicochemical

properties, yielding interdrug inconsistency in transport efficiency across the cell membrane.

Transient and reversible cellular membrane permeabilization utilizing electric pulses, namely, electroporation, can be an appealing means for drug-screening applications because it permits direct injections of newly developed cytotoxic molecules, which are inherently membrane-impermeable but can be subsequently modified to facilitate intracellular transport.^{12–14} In particular, it has been used to enhance chemotherapeutic drug efficacy for cutaneous cancers.^{15–17} Traditional electroporation drug-screening platforms have shown great promise in drug discovery; however, they have limited ability to perform cytotoxicity assays for combination therapies because their stochastic molecular delivery process precludes the determination of synergic drug dosage combinations. To overcome shortcomings of the bulk electroporation, many electroporation systems using microfluidic or nanomaterial platforms have successfully demonstrated reduction in operational costs and reagent consumptions with enhancement in molecular delivery efficiency and viability.^{18–26} Still, very few systems allow for multimolecule delivery with controlled

Received: April 22, 2014

Accepted: September 22, 2014

Published: October 7, 2014

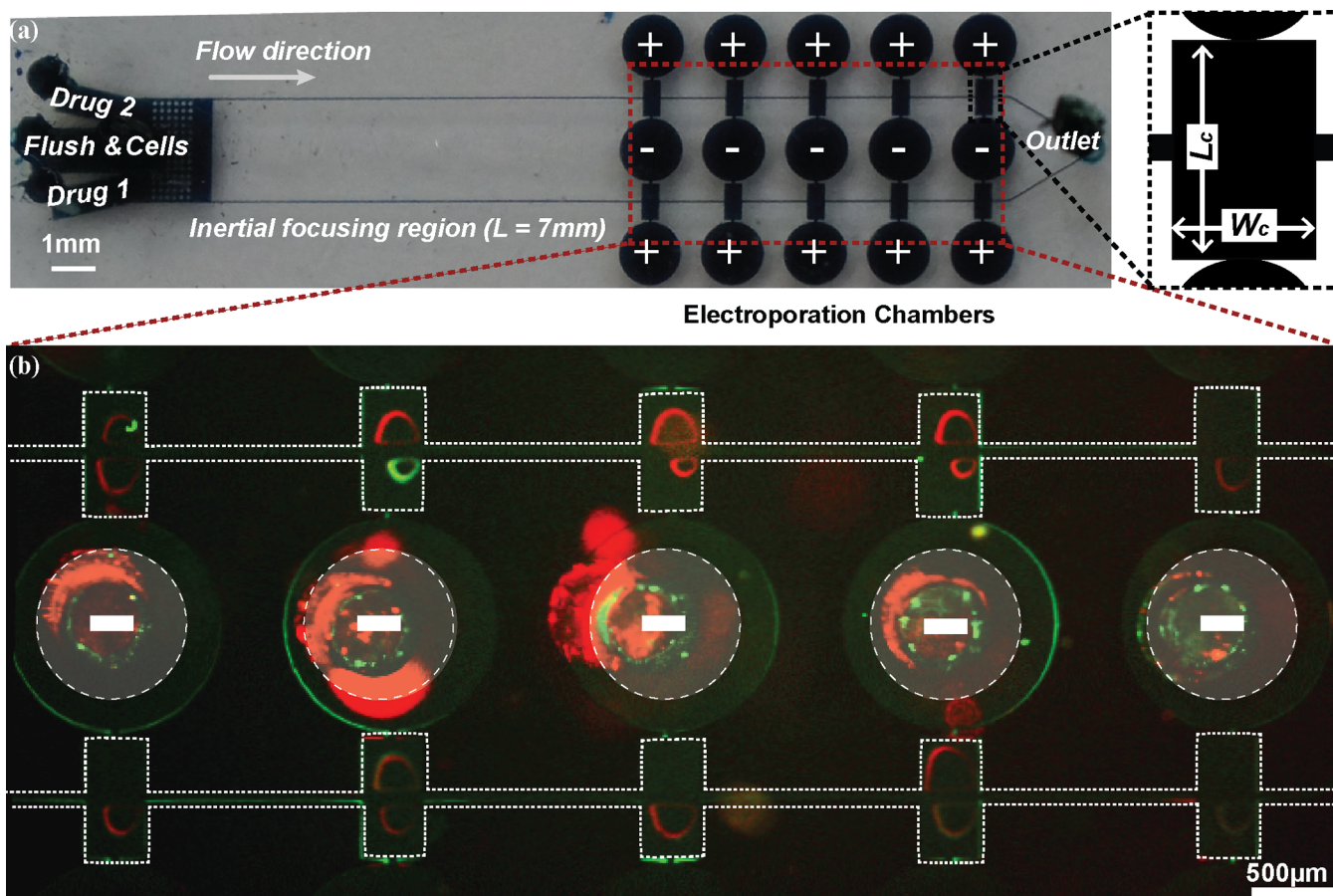


Figure 1. (a) Photograph of the microfluidic electroporation system used for sequential molecular delivery to perform direct drug cocktail analyses. The device consists of inlets for cells, drugs, and a flush solution, two straight inertial focusing channels, ten electroporation chambers with electrodes, and an outlet. The length (L_c) and the width (W_c) of individual electroporation chambers are 840 and 400 μm , respectively. (b) Representative fluorescent microscopic image illustrating parallel, dual-molecule delivery into trapped cell populations. Green and red fluorescent signals indicate successful penetration of two nucleic acid dyes, PI and YOYO-1, respectively. Image contrast has been enhanced by adjusting the look-up table (LUT).

dosages besides nontrivial off-chip collection of processed biological samples for downstream analyses.^{20,26}

Combining the advantages that microfluidics and electroporation offer, we demonstrated direct drug cocktail analysis using the vortex-assisted electroporation platform. The system enables sequential deliveries of precisely controlled amounts of multiple molecules into preselected cells, which can be subsequently released for downstream analyses. As a proof of concept, we examined the dosage-dependent cytotoxicity of chemotherapeutic drugs and an anticancerous flavonoid when those compounds were used as a single agent or in combination. The dose ratios of drug–flavonoid combinations that induce synergic and antagonistic effects were identified by systematically varying individual drug concentrations in the cytosol of cancer cells. The proposed platform has a great potential for facilitating comprehensive assessments of drug combinations directly on patients' samples upon successful integration with the label-free cell purification system.²⁷

MATERIALS AND METHODS

Cell Preparation. Metastatic breast cancer cells, MDA-MB-231 (HTB-26, ATCC), were plated at a concentration of 1×10^5 cells/mL in a volume of 10 mL per T75 tissue culture flask (CELLSTAR, Greiner Bio-One, United States) in Leibovitz's L-15 medium (Cellgro, Mediatech, Inc., United States)

supplemented with 10% (v/v) fetal bovine serum (FBS; Gibco, Life Technologies, United States) and 1% penicillin–streptomycin (Sigma-Aldrich Co., United States). These cells were incubated in a humidified incubator at 37 °C with a 0% CO₂ environment. The cells were harvested for experiments 2 days after the seeding by treating them with 0.25% trypsin–EDTA for 2 min. The cells were pelleted by centrifugation for 5 min at 200g and resuspended in the growth medium to have a final concentration of 5×10^5 cells/mL.

Device Design and Fabrication. We have parallelized the previously reported microvortex-assisted electroporation platform²⁸ to enhance the throughput without sacrificing any of its merits. The parallelized microfluidic electroporator consists of an inlet with multiple solution injection ports and coarse filters, two parallel inertial focusing channels ($L = 7$ mm, $W = 40 \mu\text{m}$, and $H = 70 \mu\text{m}$), and an outlet where two straight inertial focusing channels merge (Figure 1a). Individual straight channels consist of five electroporation chambers in series, and the electroporation chambers are placed 800 μm apart ($W_c = 400 \mu\text{m}$ and $L_c = 840 \mu\text{m}$). Individual electroporation chambers have two holes for aluminum electrodes, and two transversally adjacent chambers share the hole for negative electrodes. 2-Dimensional projection of the device was designed using AutoCAD (Autodesk, Inc., United States), and the CAD file with micropatterns was converted to a GDSII

file using LinkCAD. The micropatterns were written on a 5 in. \times 5 in. photomask blank using a laser mask writer (Heidelberg mask writer, DWL-66). The mask was developed by following the manufacturer's protocol. The casting mold was then fabricated using a negative photoresist (KMPR 1050, Microchem, United States) by following conventional photolithography procedures. The heights of the fabricated microstructures were measured using a surface profilometer (Dektak 6M, Veeco, United States). Poly(dimethylsiloxane) (PDMS; Sylgard 184 silicone elastomer kit, Dow Corning, United States) replicas were generated by following the soft lithography techniques.²⁹ PDMS was degassed for 30 min and cured for 2 h in an oven maintained at 70 °C. Cured PDMS replicas were delaminated from the mold, and solution injection ports, an outlet, and electrode insertion holes were created by using a pin vise (Pin vise set A, Syneo). Microchannels were enclosed by bonding PDMS replicas to glass slides after oxygen plasma treatments (Technics Micro-RIE, United States).

Electroporation of Target Cells for Drug Delivery. The system utilized the pneumatic flow control unit and the electrical equipment that we previously developed. Their detailed specifications²⁸ and visualized operational protocols³⁰ can be found elsewhere. In brief, the flow control unit independently and promptly pressurizes individual solution vials for rapid solution exchanges through the microfluidic system, while the electrical equipment generates high-voltage short pulses across the electroporation chambers on demand. Prior to electroporation experiments, a 15-pin aluminum electrode array³⁰ and an outlet PEEK (poly(ether ether ketone)) tube were inserted into the microfluidic device, and the electrical equipment was connected to the electrode array. Solution vials, individually containing cells, drugs, and a growth medium for flushing, were mounted into the pneumatic flow control unit, and PEEK tubes from each vial were inserted into designated inlet ports in the microfluidic electroporator. The system was flushed with the growth medium at the operating pressure of 40 psi (equivalent to a flow rate of 400 μ L/min) for 90 s prior to the target cell injection step to prime the flow speed required for cell trapping.³¹ Once the desired size and number distribution of trapped cells were attained in each cell-trapping vortex, nontrapped cells were removed from the device by switching the active solution port from the cell solution to the flush solution. Five short pulses with magnitude $V = 100$ V and pulse width $\Delta t = 30$ ms were applied promptly after the first drug solution was injected into the device. The resulting electric field strength across the electroporation chamber was $E = V/L_e = 0.7$ kV/cm. Here, $L_e = 1.5$ mm is the distance between the positive and negative electrodes that are in contact with the flowing solution. The magnitude, V , the width, Δt , and the frequency of applied electrical pulses were monitored in real time using an oscilloscope (Agilent, United States). Drug delivery doses were varied by exposing trapped cells to a single drug for incubation durations of 30, 60, and 120 s in continuous flow. For dual-drug delivery tests, trapped cells were sequentially incubated in individual drugs with various dosage combinations by systematically changing the treatment duration ratios of the two drugs (e.g., 30 s:30 s, 30 s:60 s, or 30 s:120 s). Upon completion of the drug delivery process, the treated cells were suspended in the growth medium and released from the device for downstream analysis by lowering the operating pressure to 30 psi. The collected cells were seeded in 96-well plates and cultured for 24–48 h prior to the

cytotoxicity assays. The durations for which cells were cultured prior to the cytotoxicity assays were determined on the basis of conditions previously reported for the tested drugs (bleomycin,¹⁶ gemcitabine,³² topotecan and quercetin³³).

Real-Time Molecular Delivery Visualization. The nucleic acid fluorescent dyes propidium iodide (PI) and YOYO-1 (Life Technologies, United States) were used to visualize intracellular delivery of molecules in real time, allowing prompt determination of optimum electrical parameters and electroporation efficiencies. In addition, 1 μ M bleomycin (BLM), which is fluorescently labeled with Alexa-Fluor 488 (Life Technologies), was used to identify electrical parameters required for successful drug delivery and dose control (see Figures S1 and S2, Supporting Information). For BLM–Alexa conjugation preparation, 25 μ L of Alexa-Fluor 488 (8 mM) dissolved in DMSO was added to 100 μ L of bleomycin (883 μ M) dissolved in 0.9% saline to have a molar ratio of Alexa to BLM of approximately 2:1. Then sterile water was added to make 1 mL of total reaction volume, and the mixtures were stirred at room temperature for 19 h. Unreacted residual dye molecules were removed by performing high-performance liquid chromatography (HPLC) on a system equipped with an automated fraction collector (Agilent 1100 series). The mixture was loaded onto the XTerra MS C₁₈ column (Waters, United States) using a gradient of HPLC-grade water and acetonitrile as solvents A and B (2–10% B in 10 min and 10–95% B in 5 min), respectively, with ultraviolet (UV) detection at 292 and 495 nm (see Figure S2a). The purified conjugate was dried in a SpeedVac (Thermo Fisher Scientific) at 40 °C overnight, and the dried sample was dissolved in 1 mL of sterile Dulbecco's phosphate-buffered saline (DPBS). The conjugate concentration was determined by UV-vis spectrophotometry (PerkinElmer, United States) on the basis of the BLM absorption spectrum. The molar extinction coefficient of BLM was taken as $\epsilon = 1.5 \times 10^4$ M⁻¹ cm⁻¹ at 292 nm,³⁴ and the absorption signal of Alexa 488 did not interfere with drug concentration measurements.

Drug Preparation. Dose responses of metastatic breast cancer cells were tested using chemotherapeutic drugs, bleomycin, gemcitabine, and topotecan, and an anticancerous flavonoid, quercetin, to illustrate the drug-screening capabilities of the proposed platform (Sigma-Aldrich Co., United States). Conventional drug-screening assays utilizing well plates were conducted in parallel to evaluate the performance of the proposed microfluidic system. For the microfluidic electroporation drug-screening assays, the delivery dosages were varied by changing the incubation duration (e.g., 30, 60, and 120 s) at a flow rate of 400 μ L/min where the concentrations of gemcitabine, bleomycin, topotecan, and quercetin in the injection vials were fixed at 210 μ M, 57 nM, 240 nM, and 66 nM, respectively. For control experiments using the conventional method, the concentrations of the drugs were determined such that cells would be exposed in a well plate for 24 h to the drug solute quantity that is identical to that flown through the microfluidic device during the incubation period after the electroporation. That is, the viability of cells incubated in 210, 420, and 840 μ M gemcitabine using the conventional assay was compared to that of cells treated with the drug for 30, 60, and 120 s, respectively, in the microfluidic device. Similarly, cells were incubated in bleomycin (57, 110, and 200 nM), topotecan (310, 620, and 1240 nM), and quercetin (83, 170, and 330 nM) for the control experiments.

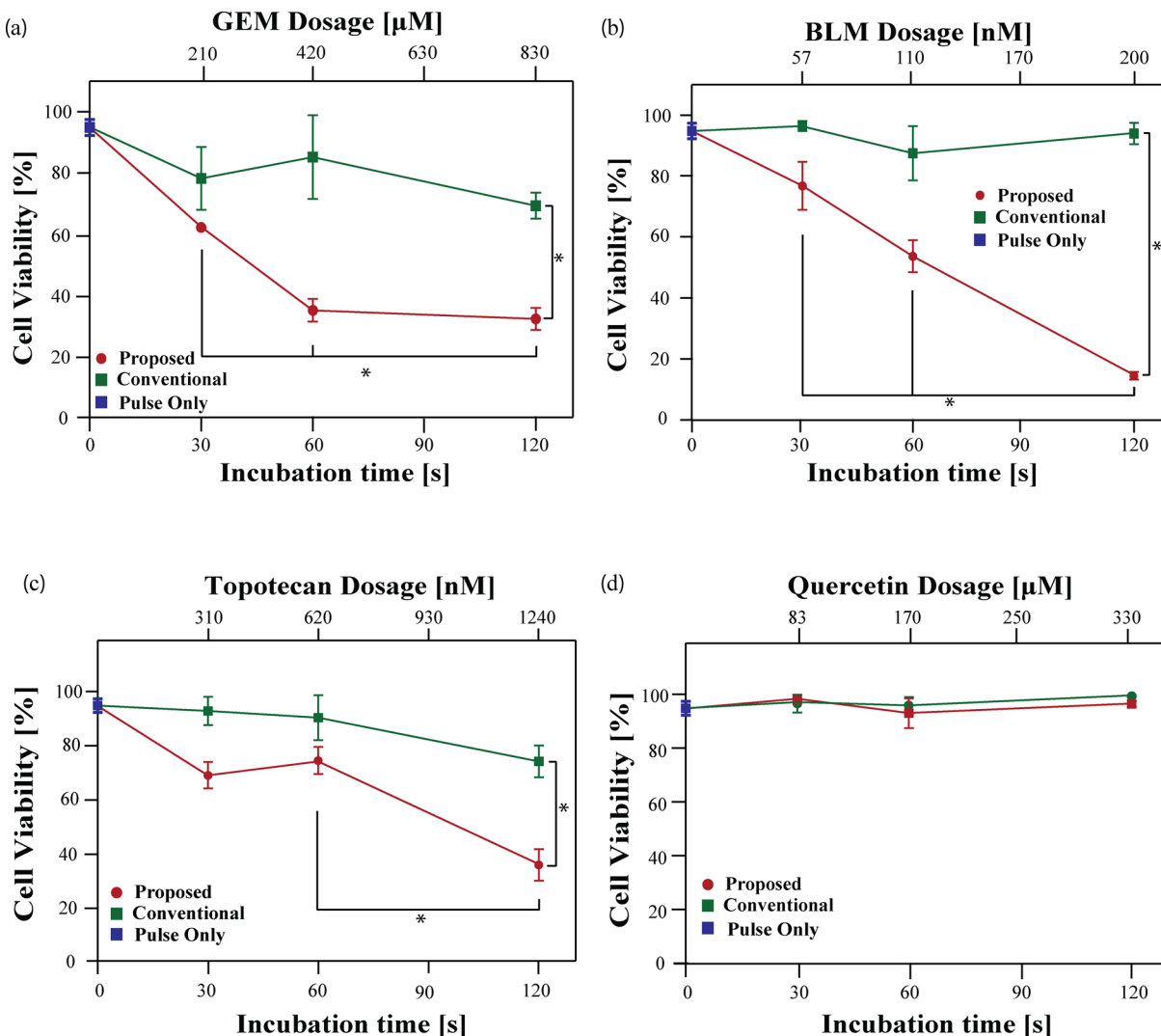


Figure 2. Dose–response curves of MDA-MB-231 cells to (a) gemcitabine (GEM), (b) bleomycin (BLM), (c) topotecan (TOP), and (d) quercetin alone. For all tested chemotherapeutic drugs, GEM, BLM, and TOP, the viability of MDA-MB-231 cells substantially decreased with increasing exposure drug concentrations, while the effect of quercetin as a single agent on cell viability was negligible and dose independent. Cells processed with the microfluidic assay exhibited a stronger dose response than those treated using the conventional assay for all tested chemotherapeutic drugs. The proposed microfluidic assay can be used to identify the effectiveness of drugs with subtle variation in the concentrations below IC_{50} values of 2 mM, 20 μ M, and 2 μ M for GEM, BLM, and TOP, respectively. The viability of electroporated cells without drug treatment is presented for comparison (blue square). An asterisk indicates $p < 0.001$. Error bars represent the standard error of measurements from three independent experiments.

Cytotoxicity Determination. The CellTiter-Glo luminescent cell viability assay (Promega, United States) was used to determine the cytotoxicity of the tested drugs. First, the correlation between the luminescent intensity and the number of viable cells for the tested cell line was established from luminescence measurements from 96-well plates containing a known quantity of viable cells (LuMate, model 4400) (see Figure S3 (Supporting Information) for the calibration curve). For cytotoxicity studies on cells treated with the drugs, all cells present in the well, regardless of their viability, were manually counted prior to addition of the CellTiter-Glo reagent to the well. The number of viable cells was determined by identifying the corresponding number of viable cells represented by the measured luminescent intensity from the calibration curve. Viability was determined by taking the ratio between the number of viable cells and the total number of treated cells present in the well. The results from the combination

treatments were analyzed to determine whether the combination was synergistic, additive, or antagonistic by calculating the combination index (CI) according to the Chou–Talalay method³⁵ using the Compusyn software (Composyn Inc., United States).

RESULTS AND DISCUSSION

In this work, a parallelized microfluidic electroporation platform was utilized for direct drug cocktail screenings. This platform renders a 10-fold enhancement in throughput in addition to all the merits that the previous single-chamber system provided.²⁸ The system's unique merits remaining uncompromised through parallelization include (i) superior viability of processed cells, (ii) on-demand injection of single substances, eliminating unforeseen adverse effects associated with drug–drug interaction prior to delivery, and (iii) sequential multimolecule delivery with highly efficient, precise,

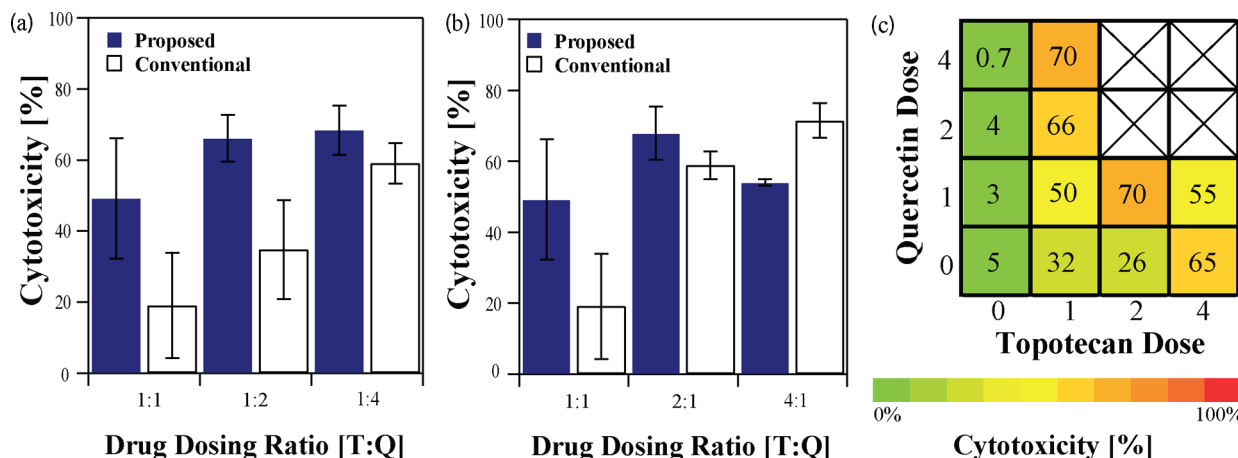


Figure 3. Dose–effect graphs for a topotecan–quercetin combination (T:Q) for MDA-MB-231 cells. (a) The anticancer effects of topotecan (30 s of exposure postelectroporation, equivalent to 310 nM) in highly invasive metastatic breast cancer cells were enhanced with increasing quercetin dosages for both assays. (b) When the concentration of quercetin for the assay was fixed at 83 nM (equivalent to 30 s of exposure postelectroporation), cells processed with the microfluidic assay exhibited sensitive dose responses of topotecan. Comparable results can be observed from the conventional assays up to T:Q = 2:1 ($p = 0.86$). However, a further increase in topotecan concentrations beyond the 2:1 ratio did not enhance cytotoxicity. (c) Heat map illustrating cytotoxic effects of the various concentrations of drugs when they were used alone or in combination. Note the dosing ratio 1:1 indicates that cells were exposed to individual drugs for 30 s each postelectroporation, which is equivalent to treating cells with 310 nM topotecan and 83 nM quercetin in well plates. Error bars represent the standard error of measurements from three independent experiments.

and independent dosage controls. The system takes advantage of the microvortex-assisted cell-trapping mechanism³¹ to preselect subpopulations of cells with a uniform size distribution, thereby allowing less variations in electroporation efficiency and enhancement in viability per given electric field strength.³⁶ Previously, we have shown that molecules ranging from small nucleic acid dyes to large naked plasmids could be introduced sequentially into preselected populations of cells as they orbit in the vortices.²⁸ Parallelization of this platform did not interfere with the sequential molecular delivery process as we confirmed through sequential delivery of the nucleic acid dyes PI and YOYO-1 into cells trapped in the 10 electroporation chambers (Figure 1b). Moreover, the molecular amount transferred into the cytosol can be modulated by varying either the electrical field strengths or molecular injection times, and intracellular concentrations of delivered substances were probed using fluorescent drug surrogates (Figures S1 and S2, Supporting Information). In a similar manner, multiple drug compounds with varied concentration ratios were delivered into cells orbiting in the electroporation chambers.

To evaluate the system's applicability toward drug-screening assays, we first assessed the dose–response characteristics of gemcitabine and bleomycin (Figure 2a,b), which have been studied extensively for electrochemotherapy for cutaneous metastasis.^{17,32} Consequently, these drugs are ideal candidates for comparative studies of the microfluidic and the conventional well-plate assay because their cytotoxic effects and optimum dosages have been well-documented. Cells treated with these drugs as single entities in well plates exhibited less significant dosing effects compared to those treated by the microfluidic device (Figure 2; Figure S2, Supporting Information). This could be attributed to the nonpermeant nature of the drugs.¹⁷ Correspondingly, higher IC₅₀ values for both drugs were obtained from the conventional assays (Table S1, Supporting Information), suggesting that IC₅₀ is strongly influenced by in-cell drug concentrations rather than accessible

drug amounts in the incubation solution. This implies that the developed system would facilitate understanding of unidentified relationships between intracellular drug concentrations and pharmacological consequences, which presumably was ascribed to conventional assays' stochastic and diffusive transmembrane transport mechanisms.

We further investigated the dose effects of a chemotherapeutic drug, topotecan, and a flavonoid with anticancer properties, quercetin, as single agents and in combination. Previously, the combination of these two substances was reported to have synergistic effects because quercetin selectively enhances cytotoxicity of chemotherapeutic drugs only in cancerous cells, suppressing off-target toxicity.^{33,37} As a single agent, topotecan dose-dependently reduced survival of cells processed using either drug-screening platform (Figure 2c). The fact that cells treated using the microfluidic platform responded more sensitively to the drug suggests that the proposed microfluidic assay can be used to identify the effectiveness of drugs with subtle variation in the concentrations. Quercetin alone, on the other hand, exhibited a negligible cytotoxic effect on cells processed with either system (Figure 2d) even at a high concentration, which is in good agreement with previous studies.^{37,38} No apparent adverse effect on cells treated with atoxic quercetin using the current system further confirms that the dose responses of the tested chemotherapeutic drugs were not altered by the electroporation and solely represent the actual cytotoxic effects of the delivered drugs.

For sequential dual-drug screenings, cells were first exposed to topotecan and quercetin for identical durations (i.e., 30 s of incubation in solutions with 240 nM topotecan and 66 nM quercetin; see Figure 3a). More than 3-fold reductions in IC₅₀ values obtained from both assays suggest that the addition of quercetin augments the cytotoxic effects of topotecan (Table S1, Supporting Information). These trends were evident at all combination ratios where a fixed concentration of topotecan was used (T:Q = 1:1, 1:2, and 1:4). The CI was computed for

all tested combinations to quantitatively evaluate the drug combinatorial effects (Table S2, Supporting Information). In such an analysis, $CI < 1$ implies synergy, $CI = 1$ represents an additive effect, and $CI > 1$ corresponds to antagonism.³⁵ Cytotoxicity assays of a fixed topotecan concentration assessed using both platforms illustrated that the drug combinations work in synergy ($CI < 1$) at all tested ratios (Figure 3a). This trend of increased drug cytotoxicity continues as the dosage of topotecan increases while that of quercetin remains unchanged ($T:Q = 2:1$). The drug ratios $T:Q = 1:1$ and $2:1$ were found to induce synergistic effects for both assays. Interestingly, the antagonistic effect ($CI = 1.11$) was detected only with the microfluidic assay at $T:Q = 4:1$, whereas the results from the conventional assay implied the synergic effect of the combination ($CI = 0.29$). Such disparity could have originated from the fact that apparent drug amounts delivered into cytosols by the microfluidic system were much greater than those by the well-plate assay. Presumably, the maximal response of the combination, E_{max} , beyond which cytotoxicity is independent of drug concentrations³⁹ has been attained for the microfluidic assay. It is also possible that the proposed system can identify elusive antagonistic drug combinations which are not detectable otherwise. Subsequent investigations are still required to reinforce this claim.

Owing to inherently small footprints of the microfluidic systems, the presented microfluidic electroporator can conduct cost-effective, single-cell-level multidrug screenings. As shown in the results, cells assayed using the presented system exhibited elevated cytotoxicity compared to those treated by the conventional well-plate method when identical amounts of drugs were used. Although the current system can screen a considerably lower number of cells than conventional methods, the channel geometry is simple and amendable to automation. Thus, the system can repeatedly process a greater number of cells to conduct an unbiased drug-screening approach to reveal serendipitous combinations of already-approved compounds. Moreover, the developed platform is anticipated to be used as a novel screening method to understand consequences of drug–target interactions for newly identified cytotoxic molecules whose transmembrane transport mechanisms are yet to be determined. Finally, the system can be readily integrated with the high-throughput vortex-assisted circulating tumor cell purification system whose clinical potentials have been demonstrated.²⁷ Successful integration will allow performance of sophisticated drug-screening analyses of patient-derived cellular models to identify interpatient variability conferring factors in drug responses.

CONCLUSION

In this work, a microscale vortex-assisted electroporation platform was implemented for direct analysis of drug cocktails. Contrary to the bulk electroporation systems, this platform does not adversely affect cell viability, suggesting that cellular responses observed from cytotoxicity assays solely represent the actual effects of the drug cocktail. Through quantitative single-drug and drug combination analyses, we were able to identify the combinational dosages of the chemotherapeutic drug and the flavonoid inducing synergistic and antagonistic effects. The system has great potential to enable drug screenings for development of personalized medicines when it is integrated with the on-chip cell purification system.²⁷

ASSOCIATED CONTENT

Supporting Information

Additional information as noted in text. This material is available free of charge via the Internet at <http://pubs.acs.org>.

AUTHOR INFORMATION

Corresponding Author

*E-mail: hur@rowland.harvard.edu. Phone: 617-497-4713.

Notes

The authors declare no competing financial interest.

ACKNOWLEDGMENTS

This work was supported by the Rowland Junior Fellow program. We would like to express our gratitude to the scientists and staff at the Rowland Institute at Harvard: Chris Stokes for his help in the development of the custom-built, computer-assisted pressure control setup, Diane Schaak, Ph.D. for her assist on performing HPLC, Winfield Hill for developing the electrical setup, Scott Bevis, Kenny Spencer and Don Rogers for machining mechanical plumbing components required for the pressure setup. Microfluidic masters were fabricated at the Center for Nanoscale Systems (CNS) at Harvard University.

REFERENCES

- (1) Meng, J.; Dai, B.; Fang, B.; Bekele, B. N.; Bornmann, W. G.; Sun, D.; Peng, Z.; Herbst, R. S.; Papadimitrakopoulou, V.; Minna, J. D.; Peyton, M.; Roth, J. A. *PLoS One* **2010**, *5*, e14124.
- (2) Méndez-Ortega, M. C.; Restrepo, S.; Rodríguez-R, L. M.; Pérez, I.; Mendoza, J. C.; Martínez, A. P.; Sierra, R.; Rey-Benito, G. J. *Virol. J.* **2010**, *7*, 369.
- (3) Williams, B. *Br. Med. J.* **2003**, *326*, 61.
- (4) Wu, Z.; Zhao, X. M.; Chen, L. *BMC Syst. Biol.* **2010**, *4* (Suppl. 2), S7.
- (5) Xu, K. J.; Song, J.; Zhao, X. M. *BMC Syst. Biol.* **2012**, *6* (Suppl. 1), S5.
- (6) Chou, T.-C. *Pharmacol. Rev.* **2006**, *58*, 621–681.
- (7) Kolishetti, N.; Dhar, S.; Valencia, P. M.; Lin, L. Q.; Karnik, R.; Lippard, S. J.; Langer, R.; Farokhzad, O. C. *Proc. Natl. Acad. Sci. U.S.A.* **2010**, *107*, 17939–17944.
- (8) Al-Lazikani, B.; Banerji, U.; Workman, P. *Nat. Biotechnol.* **2012**, *30*, 679–692.
- (9) Booth, N. L.; Sayers, T. J.; Brooks, A. D.; Thomas, C. L.; Jacobsen, K.; Goncharova, E. I.; McMahon, J. B.; Henrich, C. J. *Cancer Immunol. Immunother.* **2009**, *58*, 1229–1244.
- (10) Du, G.-S.; Pan, J.-Z.; Zhao, S.-P.; Zhu, Y.; den Toonder, J. M. J.; Fang, Q. *Anal. Chem.* **2013**, *85*, 6740–6747.
- (11) Lundholt, B. K.; Scudder, K. M.; Pagliaro, L. *J. Biomol. Screening* **2003**, *8*, 566–570.
- (12) Cemazar, M.; Parkins, C. S.; Holder, A. L.; Chaplin, D. J.; Tozer, G. M.; Sersa, G. *Br. J. Cancer* **2001**, *84*, 565–570.
- (13) Nakamura, H.; Funahashi, J. *Dev. Growth Differ.* **2013**, *55*, 15–19.
- (14) Orlowski, S.; Belehradek, J.; Paoletti, C.; Mir, L. M. *Biochem. Pharmacol.* **1988**, *37*, 4727–4733.
- (15) Gothelf, A.; Mir, L. M.; Gehl, J. *Cancer Treat. Rev.* **2003**, *29*, 371–387.
- (16) Todorovic, V.; Sersa, G.; Flisar, K.; Cemazar, M. *Radiol. Oncol.* **2009**, *43*, 264–273.
- (17) Jaroszeski, M. J.; Dang, V.; Pottinger, C.; Carlos, P.; Hickey, J.; Gilbert, R.; Heller, R. *Anti-Cancer Drugs* **2000**, *11*, 201–208.
- (18) Lee, D. W.; Choi, Y.-S.; Seo, Y. J.; Lee, M.-Y.; Jeon, S. Y.; Ku, B.; Kim, S.; Yi, S. H.; Nam, D.-H. *Anal. Chem.* **2014**, *86*, 535–542.
- (19) Adamo, A.; Arione, A.; Sharei, A.; Jensen, K. F. *Anal. Chem.* **2013**, *85*, 1637–1641.

- (20) Xie, X.; Xu, A. M.; Leal-Ortiz, S.; Cao, Y.; Garner, C. C.; Melosh, N. A. *ACS Nano* **2013**, *7*, 4351–4358.
- (21) Kim, S. K.; Kim, J. H.; Kim, K. P.; Chung, T. D. *Anal. Chem.* **2007**, *79*, 7761–7766.
- (22) Kotnik, T.; Bobanović, F.; Miklavčič, D. *Bioelectrochem. Bioenerg.* **1997**, *43*, 285–291.
- (23) Lee, W. G.; Demirci, U.; Khademhosseini, A. *Integr. Biol.* **2009**, *1*, 242–251.
- (24) Lee, W. G.; Bang, H.; Yun, H.; Min, J.; Chung, C.; Chang, J. K.; Han, D.-C. *Lab Chip* **2008**, *8*, 224–226.
- (25) Lin, J.; Chen, R.; Feng, S.; Li, Y.; Huang, Z.; Xie, S.; Yu, Y.; Cheng, M.; Zeng, H. *Biosens. Bioelectron.* **2009**, *25*, 388–394.
- (26) Boukany, P. E.; Morss, A.; Liao, W.-C.; Henslee, B.; Jung, H.; Zhang, X.; Yu, B.; Wang, X.; Wu, Y.; Li, L.; Gao, K.; Hu, X.; Zhao, X.; Hemminger, O.; Lu, W.; Lafyatis, G. P.; Lee, L. J. *Nat. Nanotechnol.* **2011**, *6*, 747–754.
- (27) Sollier, E.; Go, D. E.; Che, J.; Gossett, D. R.; O’Byrne, S.; Weaver, W. M.; Kummer, N.; Rettig, M.; Goldman, J.; Nickols, N.; McCloskey, S.; Kulkarni, R. P.; Di Carlo, D. *Lab Chip* **2014**, *14*, 63–77.
- (28) Yun, H.; Hur, S. C. *Lab Chip* **2013**, *13*, 2764–2772.
- (29) Xia, Y.; Whitesides, G. M. *Angew. Chem., Int. Ed.* **1998**, *37*, 550–575.
- (30) Vickers, D. A. L.; Hur, S. C. *J. Visualized Exp.* **2014**, DOI: 10.3791/51702.
- (31) Hur, S. C.; Mach, A. J.; Di Carlo, D. *Biomicrofluidics* **2011**, *5*, 22206.
- (32) Wang, J.; Guo, J.; Wu, S.; Feng, H.; Sun, S.; Pan, J.; Zhang, J.; Beebe, S. J. *PLoS One* **2012**, *7*, e43213.
- (33) Akbas, S. H.; Timur, M.; Ozben, T. *J. Surg. Res.* **2005**, *125*, 49–55.
- (34) Brooks, R. C.; Carnochan, P.; Vollano, J. F.; Powell, N. A.; Zweit, J.; Sosabowski, J. K.; Martellucci, S.; Darkes, M. C.; Fricker, S. P.; Murrer, B. A. *Nucl. Med. Biol.* **1999**, *26*, 421–430.
- (35) Chou, T. C.; Talalay, P. *Trends Pharmacol. Sci.* **1983**, *4*, 450–454.
- (36) Gehl, J. *Acta Physiol. Scand.* **2003**, *177*, 437–447.
- (37) Staedler, D.; Idrizi, E.; Kenzaoui, B. H.; Juillerat-Jeanneret, L. *Cancer Chemother. Pharmacol.* **2011**, *68*, 1161–1172.
- (38) Chen, C.; Zhou, J.; Ji, C. *Life Sci.* **2010**, *87*, 333–338.
- (39) Yang, R.; Niepel, M.; Mitchison, T. K.; Sorger, P. K. *Clin. Pharmacol. Ther.* **2010**, *88*, 34–38.